

# Stabilization of the Anatase Phase of $\text{Ti}_{1-x}\text{Sn}_x\text{O}_2$ ( $x < 0.5$ ) Nanofibers

Kandasami Asokan<sup>1,2</sup>, Jae Young Park<sup>1</sup>, Sunwoo Choi<sup>1</sup>, Changhwan Chang<sup>3</sup>, and Sang Sub Kim<sup>1</sup> (✉)

<sup>1</sup> School of Materials Science and Engineering, Inha University, Incheon 402–751, Republic of Korea

<sup>2</sup> Inter-University Accelerator Centre, Aruna Asaf Ali Marg, New Delhi 110067, India

<sup>3</sup> Department of Materials Test and Analysis, Research Institute of Industrial Science and Technology, Pohang 790–600, Republic of Korea

Received: 24 November 2009 / Revised: 28 January 2010 / Accepted: 1 February 2010

© The Author(s) 2010. This article is published with open access at Springerlink.com

## ABSTRACT

We experimentally investigate the stabilization of the anatase phase of  $\text{Ti}_{1-x}\text{Sn}_x\text{O}_2$  ( $x < 0.5$ ) nanofibers when synthesized by an electrospinning method. The as-spun nanofibers became nano-grained, polycrystalline nanofibers after calcination and the diameters of the nanofibers depend on Sn content. Stabilization of the anatase phase in Ti-rich compositions and incorporation of Sn ions were confirmed by X-ray diffraction, Raman, X-ray absorption near-edge structure, and photoluminescence (PL) spectroscopies. Results from the PL study also demonstrated the tunable nature of the optical properties, with the emission maximum shifting towards higher wavelength with increasing Sn concentration.

## KEYWORDS

Electrospinning, nanofiber,  $\text{Ti}_{1-x}\text{Sn}_x\text{O}_2$ , X-ray absorption near-edge structure (XANES)

## 1. Introduction

One-dimensional (1-D) nanostructured metal oxides like  $\text{TiO}_2$ ,  $\text{ZnO}$ , and  $\text{SnO}_2$  exhibit various novel physical and chemical properties with potential applications in nanoelectronics [1–3]. Several methods have been used to synthesize these oxides in the form of nanoparticles, nanotubes, nanowires, nanorods, and nanofibers [1]. Binary oxide semiconductors constitute an important class of sensing materials used in gas sensors because they are cost-effective, chemically inert, mechanically hard, and thermally heat-resistant, and therefore can be used in a harsh environment and are reliable over a long period. Electrospinning is one of the several methods available for the synthesis

of 1-D nanofibers. Recently,  $\text{TiO}_2$ - and  $\text{SnO}_2$ -based nanofibers were fabricated by electrospinning techniques and several studies focused on their potential applications in areas such as gas sensing, photoelectrochemical applications, solar cells, and photocatalytic activity [4–8].

$\text{SnO}_2$ -based gas sensors are now commercially available. But  $\text{SnO}_2$  has the major disadvantage of thermal instability and degradation in its electrical properties upon prolonged thermal treatment [9].  $\text{TiO}_2$ -based gas sensors have high thermal and chemical stability, but can operate only at relatively high temperatures (400 °C).  $\text{SnO}_2$  exhibits better electrical conductivity compared with  $\text{TiO}_2$ . It is also possible to control the porosity in these oxides, which

Address correspondence to sangsub@inha.ac.kr

is extremely important for a wide range of applications. When these two materials are coupled, it is expected that the photogenerated electrons from  $\text{TiO}_2$  will be transferred to  $\text{SnO}_2$  [10]. Many investigations have found that when these two oxides are coupled by suitable preparation methods, one can optimize their gas sensing or tune other properties required for various applications [4, 5, 9, 11–21].

From the electronic structure point of view, these oxides have different band gap energies ( $E_g$ ): 3.8 eV ( $\text{SnO}_2$ ) and 3.2 eV ( $\text{TiO}_2$ ) [22]. Thus, when these oxides are mixed the conduction band of  $\text{SnO}_2$  will act as a sink for electrons and the valence band of  $\text{TiO}_2$  will accumulate holes, thereby increasing the efficiency of charge separation [12]. In other words, one can tune their band gap by varying the stoichiometry as per specific requirements. It is well documented that the pure anatase phase shows better photocatalytic activity and can foster biocompatibility. Structurally, these oxides possess tetragonal crystal structures. Sn and Ti ions are isovalent with the same coordination numbers. However,  $\text{SnO}_2$  has a rutile tetragonal crystal structure with no anatase analog [13]. Therefore, research has focused on the synthesis of  $\text{Ti}_{1-x}\text{Sn}_x\text{O}_2$  compounds with the rutile-type structure over the entire range of solid solubility above 1450 °C [13]. These oxides have been prepared in various forms using several methods including sol–gel reactions, co-precipitation, solid-state reactions, and sputtering [8, 9, 11–21]. Since anatase phase  $\text{TiO}_2$  exhibits substantially higher photoactivity than the rutile phase, it is desirable to synthesize  $\text{Ti}_{1-x}\text{Sn}_x\text{O}_2$  in the anatase phase. However, this imposes constraints on the preparation conditions and also a limitation on the Sn content, with  $x$  being less than 0.5.

In this study, we investigated the stabilization of anatase-structured  $\text{Ti}_{1-x}\text{Sn}_x\text{O}_2$  ( $x < 0.5$ ) nanofibers synthesized by an electrospinning method. These nanofibers were characterized before and after calcination by various experimental techniques in order to understand their morphology, phase formation, crystallinity, and optical properties.

## 2. Experimental

Polyvinyl acetate (PVAc) with a molecular mass of ~850 000, titanium tetrakisopropoxide ( $\text{Ti(O}^{\prime}\text{Pr})_4$ ) and

tin chloride dihydrate ( $\text{SnCl}_2 \cdot 2\text{H}_2\text{O}$ ) were used as the precursor materials for synthesis of the nanofibers. The electrospinning solution was prepared by following a standard procedure and loaded into a glass syringe, equipped with a 21-gauge stainless steel needle [7, 10]. A positive voltage of 15 kV was applied to the needle while the metal collector was grounded. At the same time, a negative voltage was applied to the metal collector to accelerate the electrospinning process. The electrospun nanofibers were distributed uniformly over Si wafers placed on the metal collector. Thermogravimetric–differential thermal analysis (TG-DTA) was used to determine the calcination temperature required to remove water and other decomposable organic matter present in as-spun nanofibers. The as-spun nanofibers were calcined at various temperatures for varying time in an oxygen atmosphere using a tube-type furnace to obtain the required phase and morphology.

The morphological features and the phase purity of the synthesized nanofibers were examined by field-emission scanning electron microscopy (FE-SEM), energy dispersive X-ray analysis (EDX), transmission electron microscopy (TEM), X-ray diffraction (XRD), Raman, and photoluminescence (PL) spectroscopies. To confirm the anatase phase of these oxide nanofibers, X-ray absorption near-edge structure (XANES) measurements at the Ti K-edge were carried out at the Pohang Accelerator Laboratory, Korea using 8C1 POSCO beamline in fluorescence mode by following a standard procedure for such measurements.

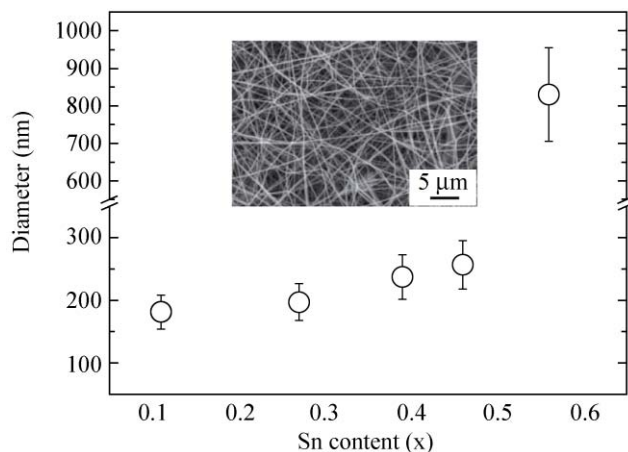
## 3. Results and discussion

Figure 1 shows the variation of the diameter of  $\text{Ti}_{1-x}\text{Sn}_x\text{O}_2$  nanofibers, measured from the FE-SEM images of corresponding nanofibers, as a function of Sn content. The diameter of the nanofibers increases with Sn content. A typical FE-SEM image of as-spun  $\text{Ti}_{1-x}\text{Sn}_x\text{O}_2$  ( $x = 0.1$ ) nanofibers is shown in the inset of Fig. 1. It displays almost smooth fibrous morphology and similar features were observed previously for  $\text{TiO}_2$  and  $\text{SnO}_2$  nanofibers [7, 10, 22–24]. The thermal behavior of  $\text{Ti}_{1-x}\text{Sn}_x\text{O}_2$  nanofibers was investigated by TG-DTA and these results were used to determine the optimum calcination temperature. The DTA curve obtained from



typical as-spun nanofibers showed two exothermic peaks: one at ~250 °C and the other at ~470 °C. The decomposition of organic matter and evaporation of water occurs at these temperatures. All the as-spun nanofibers were found to be amorphous in nature and typically became crystalline after calcination at 600 °C. Our previous study showed that the optimum calcination conditions (600 °C for 6 h) resulted in a well-defined anatase phase of TiO<sub>2</sub> [24]. Since the present study is focused on Ti rich phases, the optimum calcination temperature is also expected to be close to this value. Previous studies also showed that the activity of the photocatalysts was improved by annealing at a high temperature, after selecting the optimal annealing conditions required to obtain a highly crystalline anatase phase with no phase transformation to a rutile phase [8, 24, 25].

Figure 2 depicts the morphological evolution of Ti<sub>1-x</sub>Sn<sub>x</sub>O<sub>2</sub> ( $x = 0.1, 0.3, 0.4, 0.5, 0.6$ , and  $0.7$ ) nanofibers, after calcination at 600 °C in O<sub>2</sub> for 6 h. Note that nanofibers were formed up to the composition with  $x = 0.5$ . However, above this level, Sn rich clusters were formed probably due to structural instability. It is also evident that the diameter of the nanofibers increases with Sn content. A high-resolution TEM lattice image of Ti<sub>1-x</sub>Sn<sub>x</sub>O<sub>2</sub> ( $x = 0.1$ ) nanofibers is shown in Fig. 2(g). The inset of Fig. 2(g) shows a selected area electron diffraction pattern, indicating the



**Figure 1** Variation of the diameter of Ti<sub>1-x</sub>Sn<sub>x</sub>O<sub>2</sub> nanofibers as a function of Sn content. The inset shows a typical FE-SEM image of as-spun nanofibers. They are uniform, smooth, and show fibrous morphology

polycrystalline nature of the nanofibers. A dark-field TEM image with the corresponding EDX elemental mapping of the same nanofiber region, indicating spatial distribution of O (blue), Sn (green), and Ti (red), is shown in Fig. 2(h). Similar behaviors were observed for all compositions up to  $x = 0.5$  and are not shown here to avoid repetition.

The XRD patterns of Ti<sub>1-x</sub>Sn<sub>x</sub>O<sub>2</sub> ( $x = 0.4$ ) nanofibers calcined at temperatures between 500 °C and 800 °C for 6 h in O<sub>2</sub> are shown in Fig. 3(a). After calcination, there is an increase in the intensities of XRD peaks and the patterns correspond to an anatase phase. The XRD results indicate the formation of an anatase phase for nanofibers calcined up to 800 °C in O<sub>2</sub> [12]. XANES has been previously used as a fingerprint to identify different phases of TiO<sub>2</sub> [26]. To confirm the formation of an anatase phase in Ti<sub>1-x</sub>Sn<sub>x</sub>O<sub>2</sub> ( $x = 0.4$ ) nanofibers, XANES measurements at the Ti K-edge were carried out. Figure 3(b) shows the XANES spectra of both as-spun and calcined nanofibers of Ti<sub>1-x</sub>Sn<sub>x</sub>O<sub>2</sub> ( $x = 0.4$ ). The as-spun nanofiber sample shows a noisy spectrum with a broad pre-edge, and the main absorption edge implying the presence of an amorphous material consisting of a mixed phase of many Ti-containing compounds. In contrast, the calcined sample shows pre-edge features ( $P_1$ ,  $P_2$ , and  $P_3$ ) and also main absorption features  $B_1$  and  $C_1$  along with fine structure in the low-energy shoulder region. These features have been commonly observed for the anatase phase of TiO<sub>2</sub>. There is no high intensity peak at 4992 eV, implying the absence of a rutile phase [26, 27]. Figure 3(c) shows a representative Raman spectrum of Ti<sub>1-x</sub>Sn<sub>x</sub>O<sub>2</sub> ( $x = 0.4$ ). It is known that the anatase phase of TiO<sub>2</sub> has six Raman modes:  $A_{1g} + 2B_{1g} + 3E_g$  [3, 23]. Five phonon modes at 142, 195, 397, 520, and 636 cm<sup>-1</sup> are observed in the spectrum [25]. One of the phonon modes,  $B_{1g}$ , is not observed. Compared with pure TiO<sub>2</sub>, there is a slight shift in the frequencies of these modes and also a reduction in intensity. This is expected due to incorporation of Sn which distorts the pure anatase TiO<sub>2</sub> structure. The absence of modes assigned to the rutile structure at 454 and 610 cm<sup>-1</sup> again confirms the stabilization of the anatase phase in this material [22, 25], which is consistent with the above XRD results.

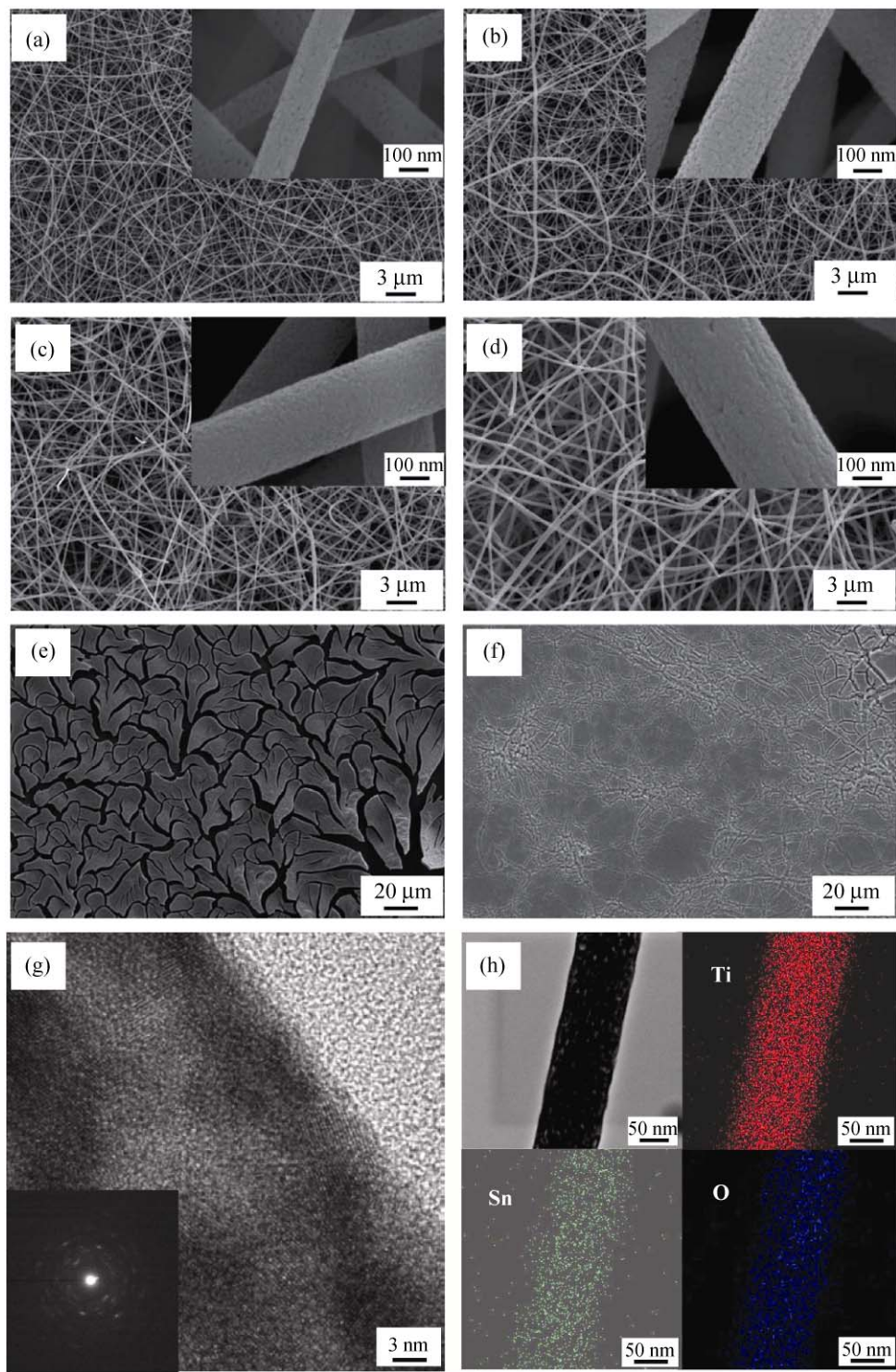


**Figure 2** FE-SEM images of  $\text{Ti}_{1-x}\text{Sn}_x\text{O}_2$  nanofibers calcined at  $600^\circ\text{C}$  in  $\text{O}_2$  for 6 h: (a)  $x = 0.1$ , (b) 0.3, (c) 0.4, (d) 0.5, (e) 0.6, and (f) 0.7. Note that nanofibers are formed up to the composition with  $x = 0.5$ . But above this critical level, instead of nanofibers, Sn rich clusters evolve. (g) High-resolution TEM lattice image taken from an individual  $\text{Ti}_{1-x}\text{Sn}_x\text{O}_2$  ( $x = 0.1$ ) nanofiber. The inset shows a selected area electron diffraction pattern, indicating a polycrystalline nature. (h) Dark-field TEM image with the corresponding EDX elemental mapping of the same nanofiber region, indicating spatial distribution of O (blue), Sn (green), and Ti (red)

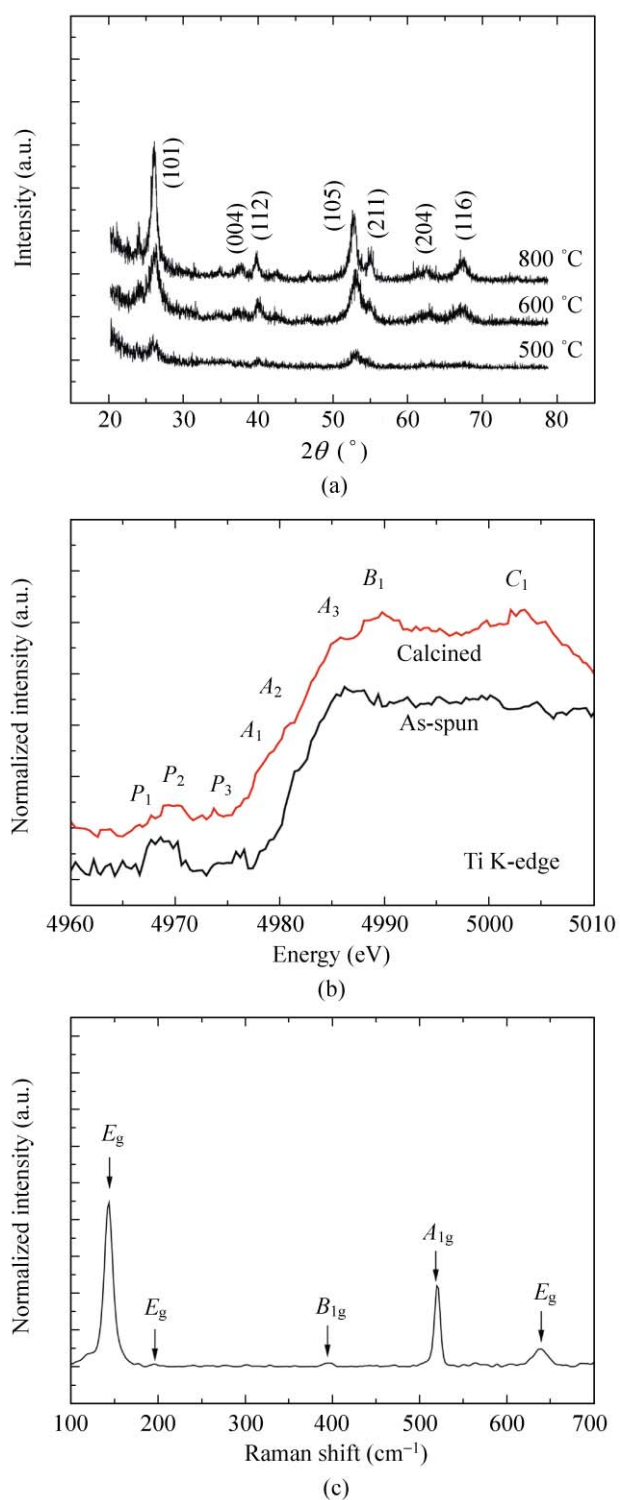


**Figure 3** (a) Typical XRD patterns of  $\text{Ti}_{1-x}\text{Sn}_x\text{O}_2$  ( $x = 0.4$ ) nanofibers calcined at 500, 600, and 800 °C for 6 h in  $\text{O}_2$ . Note that as-spun nanofibers are amorphous and become crystalline after calcination above 500 °C. (b) XANES spectrum at the Ti K-edge of  $\text{Ti}_{1-x}\text{Sn}_x\text{O}_2$  ( $x = 0.4$ ) nanofibers calcined at 600 °C. For comparison, an XANES spectrum obtained from as-spun nanofibers is included. (c) Raman spectrum of the same calcined nanofibers

One of the experimental techniques to understand the optical properties of semiconductors is PL spectroscopy. The PL spectrum originates from band–band transitions and excitonic transitions. Depending upon the band gap, surface defects, and calcination effects, different emission peaks are observed for different phases. The PL spectrum of an anatase phase is expected to be quite different from that of a rutile phase because of their significant structural differences [28]. This fact is useful in characterizing such oxide nanofibers. Figure 4 shows the PL spectra of  $\text{Ti}_{1-x}\text{Sn}_x\text{O}_2$  nanofibers of various compositions ( $x < 0.5$ ) calcined at 600 °C in  $\text{O}_2$  for 6 h. A broad emission band in the visible region peaking at about 550 nm is observed in the spectrum of the material with  $x = 0.5$ . This is attributed to the radiative recombination of self-trapped excitons [24, 28]. In the basic cell, each  $(\text{Ti}, \text{Sn})^{4+}$  cation is surrounded by an octahedron of six  $\text{O}^{2-}$  ions. Due to the high surface-to-volume ratio, oxygen vacancies are easily formed in nanofibers resulting in structural defects at Ti centers in the basic cell of  $\text{Ti}_{1-x}\text{Sn}_x\text{O}_2$ . PL transitions associated with such structural defects in rutile phases are expected to arise at 820 nm and their absence again confirms that these nanofibers have a pure anatase structure [24, 28]. Generally, oxygen vacancies are known to be the most common defects and usually act as radiative centres in luminescence processes. Generally, the oxygen vacancies ( $\text{Vo}$ ) in semiconductors are present in three different charge states: neutral ( $\text{Vo}^0$ ), and charged  $\text{Vo}^+$  and  $\text{Vo}^{++}$ . As  $\text{Vo}^0$  is a very shallow donor, most oxygen vacancies will be in a paramagnetic state under flat-band conditions [28–31]. The origin of the green emission in bulk materials is still debatable and some authors attribute it to oxygen vacancies while others attribute it to Ti or Sn interstitials [31]. However, it is widely accepted that the origin of the green emission band in the PL spectrum of  $\text{Ti}(\text{Sn})\text{O}_2$  nanofibers is assigned to the recombination of electrons in the single occupied oxygen vacancies with photoexcited holes [28–31]. As the concentration of Sn increases, the emission maximum shifts towards higher wavelength. Previous studies have shown that an increase in temperature is likely to create more O vacancies whilst calcination for

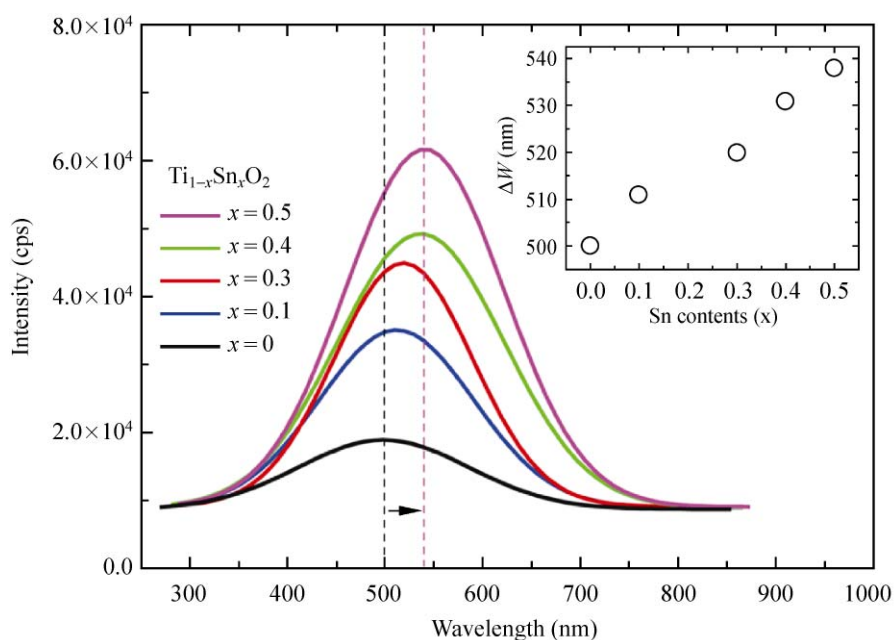


**Figure 4** Room temperature PL spectra of  $\text{Ti}_{1-x}\text{Sn}_x\text{O}_2$  ( $x < 0.5$ ) nanofibers calcined at  $600\text{ }^\circ\text{C}$  for 6 h. The inset shows the variation in the peak position with Sn concentration

longer durations results in fewer oxygen vacancies. It is also known that the PL spectra of nanostructures are usually broad and often asymmetric. The degree of crystallinity improves with the increase of calcination temperature above  $400\text{ }^\circ\text{C}$ . Investigation of the thermal stability or grain growth behavior is therefore important from the technological point of view as well as for scientific interest.

As mentioned above in the Introduction,  $\text{SnO}_2$  and  $\text{TiO}_2$  have been extensively studied due to their potential use in solar cells and as photocatalysts [11]. The principles of these applications are quite similar, being based on light absorption, light-electron conversion, and electron transportation processes. To enhance the light conversion efficiency and improve the performance of the solar cells or photocatalysts, it is necessary to: (a) achieve high external quantum yields across a broad visible light spectrum, (b) increase the diffusion length of electrons within the nanocrystalline materials, and (c) speed up the electron transport process [11, 32]. As  $\text{TiO}_2$  and  $\text{SnO}_2$  materials have different band gaps, their composites cover a broader light spectrum than the individual materials. Hence, our results showing stabilization of the anatase phase

of  $\text{Ti}(\text{Sn})\text{O}_2$  in the nanofiber form have significant relevance for applications of the materials in solar cells and also as photocatalysts. Compared with bulk materials, the specific surface area, and surface-to-volume ratios increase dramatically in the nanofibers. A high surface area is beneficial in many  $\text{Ti}(\text{Sn})\text{O}_2$ -based devices, as it facilitates reaction/interaction between the device and the interacting media, since this mainly occurs on the surface or at the interface and strongly depends on the surface area of the material. As the most promising photocatalyst,  $\text{Ti}(\text{Sn})\text{O}_2$  materials may play an important role in helping to solve many serious environmental and pollution challenges. Stabilization of the anatase phase of  $\text{Ti}(\text{Sn})\text{O}_2$  is likely to enhance research activity aimed at tackling the energy crisis through effective utilization of solar energy based on photovoltaic and water-splitting devices. Breakthroughs in the preparation, modification, and applications of  $\text{Ti}(\text{Sn})\text{O}_2$  should further promote research and development efforts to tackle the environmental and energy challenges we are currently facing. In addition,  $\text{TiO}_2$  nanomaterials are transparent in the visible light region. The observed modifications of the optical properties of

Ti(Sn)O<sub>2</sub> nanomaterials, are closely related to the Sn doping. Our results facilitate the understanding and further improvement of current and practical Sn-doped TiO<sub>2</sub> nanotechnology. The major advantages of the nanofibers are their increased contact area and surface area which are critical parameters for green chemistry applications. Thus, the properties of the nanofiber surface reflect the potential for developments in catalysis, surface science, and electrochemistry [32].

#### 4. Conclusions

The anatase phase of Ti<sub>1-x</sub>Sn<sub>x</sub>O<sub>2</sub> ( $x < 0.5$ ) has been stabilized in solid polycrystalline nanofibers. XRD, PL, Raman, and XANES measurements confirm both the incorporation of Sn and stabilization of the anatase structure. These results may open up the possibility of applications of anatase phase Ti<sub>1-x</sub>Sn<sub>x</sub>O<sub>2</sub> ( $x < 0.5$ ) nanofibers in nanoelectronics.

#### Acknowledgements

This work was supported by the Korea Science and Engineering Foundation (KOSEF) grant funded by the Ministry of Education, Science, and Technology (MEST) (No. M2AN01). One of the authors (K. A.) appreciates the support of the Brainpool Program during his stay in Inha University.

**Open Access:** This article is distributed under the terms of the Creative Commons Attribution Noncommercial License which permits any noncommercial use, distribution, and reproduction in any medium, provided the original author(s) and source are credited.

#### References

- [1] Kuchibhatla, S. V. N. T.; Karakoti, A. S.; Bera, D.; Seal, S. One dimensional nanostructured materials. *Prog. Mater. Sci.* **2007**, *52*, 699–913.
- [2] Noh, J. H.; Lee, S. H.; Lee, S. W.; Jung, H. S. Influence of ZnO seed layers on charge transport in ZnO nanorod-based dye-sensitized solar cells. *Electron. Mater. Lett.* **2008**, *4*, 71–74.
- [3] Park, J. Y.; Kim, S. S. Growth of nanograins in electrospun ZnO nanofibers. *J. Am. Ceram. Soc.* **2009**, *92*, 1691–1694.
- [4] Choi, S. W.; Park, J. Y.; Lee, J. W.; Kim, S. S. Synthesis of SnO<sub>2</sub>–ZnO core–shell nanofibers via a novel two-step process and their gas sensing properties. *Nanotechnology* **2009**, *20*, 465603.
- [5] Park, J. Y.; Choi, S. W.; Lee, J. W.; Lee, C.; Kim, S. S. Synthesis and gas sensing properties of TiO<sub>2</sub>–ZnO core–shell nanofibers. *J. Am. Ceram. Soc.* **2009**, *92*, 2551–2554.
- [6] Park, J. Y.; Kim, S. S. Effects of processing parameters on the synthesis of TiO<sub>2</sub> nanofibers by electrospinning. *Met. Mater. Int.* **2008**, *15*, 95–99.
- [7] Yuan, Z. Y.; Su, B. L. Titanium oxide nanotubes, nanofibers and nanowires. *Colloids Surf. A: Physicochem. Eng. Asp.* **2004**, *241*, 173–183.
- [8] Liu, Z.; Sun, D. D.; Guo, P.; Leckie, J. O. An efficient bicomponent TiO<sub>2</sub>/SnO<sub>2</sub> nanofiber photocatalyst fabricated by electrospinning with a side-by-side dual spinneret method. *Nano Lett.* **2007**, *7*, 1081–1085.
- [9] Oliveira, M. M.; Schnitzler, D. C.; Zarbin, A. J. G. (Ti,Sn)O<sub>2</sub> mixed oxides nanoparticles obtained by the sol–gel route. *Chem. Mater.* **2003**, *15*, 1903–1909.
- [10] Dharmaraj, N.; Kim, C. H.; Kim, K. W.; Kim, H. Y.; Suh, E. K. Spectral studies of SnO<sub>2</sub> nanofibres prepared by electrospinning method. *Spectrochim. Acta A: Mol. Biomol. Spectrosc.* **2006**, *64*, 136–140.
- [11] Grätzel, M. Photoelectrochemical cells. *Nature* **2001**, *414*, 338–344.
- [12] El-Maghraby, E. M.; Nakamura, Y.; Rengakuji, S. Composite TiO<sub>2</sub>–SnO<sub>2</sub> nanostructured films prepared by spin-coating with high photocatalytic performance. *Catal. Commun.* **2008**, *9*, 2357–2360.
- [13] Chaisan, W.; Yimnirun, R.; Ananta, S.; Cann, D. P. The effects of the spinodal microstructure on the electrical properties of TiO<sub>2</sub>–SnO<sub>2</sub> ceramics. *J. Solid State Chem.* **2005**, *178*, 613–620.
- [14] Liu, Z.; Pan, K.; Liu, M.; Wang, M.; Lu, Q.; Li, J.; Bai, Y.; Li, T. Al<sub>2</sub>O<sub>3</sub>-coated SnO<sub>2</sub>/TiO<sub>2</sub> composite electrode for the dye-sensitized solar cell. *Electrochim. Acta* **2005**, *50*, 2583–2589.
- [15] Zhou, M.; Yu, J.; Liu, S.; Zhai, P.; Jiang, L. Effects of calcination temperatures on photocatalytic activity of SnO<sub>2</sub>/TiO<sub>2</sub> composite films prepared by an EPD method. *J. Hazard. Mater.* **2008**, *154*, 1141–1148.
- [16] Chinarro, E.; Moreno, B.; Jurado, J. R. Combustion synthesis and EIS characterization of TiO<sub>2</sub>–SnO<sub>2</sub> system. *J. Eur. Ceram. Soc.* **2007**, *27*, 3601–3604.
- [17] Xiong, C. R.; Balkus, K. J. Mesoporous molecular sieve derived TiO<sub>2</sub> nanofibers doped with SnO<sub>2</sub>. *J. Phys. Chem. C* **2007**, *111*, 10359–10367.

- [18] Lin, C. F.; Wu, C. H.; Onn, Z. N. Degradation of 4-chlorophenol in  $\text{TiO}_2$ ,  $\text{WO}_3$ ,  $\text{SnO}_2$ ,  $\text{TiO}_2/\text{WO}_3$  and  $\text{TiO}_2/\text{SnO}_2$  systems. *J. Hazard. Mater.* **2008**, *154*, 1033–1039.
- [19] Pilkenton, S.; Raftery, D. Solid-state NMR studies of the adsorption and photooxidation of ethanol on mixed  $\text{TiO}_2$ – $\text{SnO}_2$  photocatalysts. *Solid State Nucl. Magn. Reson.* **2003**, *24*, 236–253.
- [20] Subasri, R.; Shinohara, T. Investigations on  $\text{SnO}_2$ – $\text{TiO}_2$  composite photoelectrodes for corrosion protection. *Electrochem. Commun.* **2003**, *5*, 897–902.
- [21] Shifu, C.; Lei, C.; Shen, G.; Gengyu, C. The preparation of coupled  $\text{SnO}_2/\text{TiO}_2$  photocatalyst by ball milling. *Mater. Chem. Phys.* **2006**, *98*, 116–120.
- [22] Nuansing, W.; Nimmuang, S.; Jarernboon, W.; Maensiri, S.; Seraphin, S. Structural characterization and morphology of electrospun  $\text{TiO}_2$  nanofibers. *Mater. Sci. Eng. B* **2006**, *131*, 147–155.
- [23] Li, D.; Xia, Y. Electrospinning of nanofibers: Reinventing the wheel? *Adv. Mater.* **2006**, *16*, 1151–1170.
- [24] Park, J. Y.; Choi, S. W.; Asokan, K.; Kim, S. S. Growth of nanograins in  $\text{TiO}_2$  nanofibers synthesized by electrospinning. *J. Nanosci. Nanotechnol.* **2010**, in press.
- [25] Qiu, Y.; Yu, J. Synthesis of titanium dioxide nanotubes from electrospun fiber templates. *Solid State Commun.* **2008**, *148*, 556–558.
- [26] Chen, X.; Mao, S. S. Titanium dioxide nanomaterials: Synthesis, properties, modifications, and applications. *Chem. Rev.* **2007**, *107*, 2891–2959.
- [27] Manzini, I.; Antonioli, G.; Lottici, P. P.; Gnappi, G.; Montenero, A. X-ray absorption study of titanium coordination in sol–gel derived  $\text{TiO}_2$ . *Physica B* **1995**, *208–209*, 607–608.
- [28] Tang, H.; Berger, H.; Schmid, P. E.; Levy, F. Photoluminescence in  $\text{TiO}_2$  anatase single crystals. *Solid State Commun.* **1993**, *87*, 847–850.
- [29] He, H.; Wu, T. H.; Hsin, C. L.; Li, K. M.; Chen, L. J.; Chueh, Y. L.; Chou, L. J.; Wang, Z. L. Beaklike  $\text{SnO}_2$  nanorods with strong photoluminescent and field-emission properties. *Small* **2006**, *2*, 116–120.
- [30] Xiang, X.; Zu, X. T.; Zhu, S.; Wang, L. M.; Shutthanandan, V.; Nachimuthu, P.; Zhang, Y. Photoluminescence of  $\text{SnO}_2$  nanoparticles embedded in  $\text{Al}_2\text{O}_3$ . *J. Phys. D: Appl. Phys.* **2008**, *41*, 225102.
- [31] Jang, Y. R.; Yoo, K. H. Green emission from  $\text{ZnO}$  thin films. *J. Korean Phys. Soc.* **2008**, *53*, 110–114.
- [32] Ramakrishna, S.; Fujihara, K.; Teo, W. E.; Lim, T. C.; Ma, Z. *An Introduction to Electrospinning and Nanofibers*; World Scientific Publishing Company: Singapore, 2005.

